

Giant Metrewave Radio Telescope detections of two high-opacity HI 21 cm absorbers at $z \approx 1.2$

ADITYA CHOWDHURY,¹ NISSIM KANEKAR,¹ AND JAYARAM N. CHENGALUR¹

¹*National Centre for Radio Astrophysics,
Tata Institute of Fundamental Research,
Pune 411007, India.*

ABSTRACT

We report the discovery of two remarkable high-opacity HI 21 cm absorbers against low-luminosity active galactic nuclei (AGNs), at $z = 1.2166$ towards J0229+0044 and at $z = 1.1630$ towards J0229+0053. The absorbers were detected in an unbiased Giant Metrewave Radio Telescope survey for HI 21 cm absorption against radio sources in the DEEP2 survey fields, covering $z \approx 0.73 - 1.53$, and including sources without known redshifts. The velocity-integrated HI 21 cm optical depths are $(74.2 \pm 7.8) \text{ km s}^{-1}$ (J0229+0044) and $(78.41 \pm 0.81) \text{ km s}^{-1}$ (J0229+0053), higher than that of any known redshifted HI 21 cm absorber at $z > 0.12$, and implying high HI column densities, $> 10^{22} \text{ cm}^{-2}$. The emission redshift of J0229+0044 is consistent with the HI 21 cm absorption redshift, while the strength and velocity spread of the absorption against J0229+0053 suggest that it too arises from gas in the AGN environment: both absorbers are thus likely to be “associated” systems. The two AGNs have low rest-frame 1.4 GHz radio and 1215 Å ultraviolet luminosities ($\lesssim 10^{26.1} \text{ W Hz}^{-1}$ and $\lesssim 10^{21.7} \text{ W Hz}^{-1}$, respectively), both significantly lower than the typical luminosities of AGNs against which HI 21 cm searches have hitherto been carried out at $z \gtrsim 1$. The paucity of HI 21 cm absorbers at $z \gtrsim 1$ may be due to a luminosity bias in high- z AGN samples that have been searched for HI 21 cm absorption, where the high AGN ultraviolet luminosity affects physical conditions in its environment, ionizing the neutral hydrogen.

Keywords: Active galactic nuclei — Radio spectroscopy — Neutral hydrogen clouds

1. INTRODUCTION

For radio-loud active galactic nuclei (AGNs), studies of “associated” HI 21 cm absorption by neutral atomic hydrogen (HI) in the AGN environment provide an interesting probe of physical conditions in the vicinity of AGNs (see [Morganti & Oosterloo 2018](#), for a recent review). For example, the strength of the HI 21 cm absorption yields information on the HI column density N_{HI} and the gas spin temperature T_s , and how these are affected by proximity to the AGN. The HI 21 cm absorption kinematics, relative to the AGN, can be used to determine whether the HI is infalling (redshifted) or outflowing (blueshifted), and thus, to infer the importance of AGN fuelling and feedback at different cosmological epochs (e.g. [van Gorkom et al. 1989](#); [Vermeulen et al. 2003](#); [Morganti et al. 2003, 2016](#)). Very long baseline interferometric HI 21 cm absorption studies can be used to track the influence of the AGN jets on the gas, and the driving of high-velocity outflows (e.g. [Oosterloo et al. 2000](#); [Morganti et al. 2013](#)). The detection rates of HI 21 cm absorption in different AGN types can provide information on the evolutionary history of AGNs, and on AGN unification schemes (e.g. [Vermeulen et al. 2003](#)). High-opacity HI 21 cm absorbers are also good candidates for searches for radio molecular absorption (e.g. [Wiklind & Combes 1994](#); [Kanekar et al. 2005](#); [Allison et al. 2019](#)), which can be used to probe fundamental constant evolution on cosmological timescales (e.g. [Kanekar 2011](#); [Kanekar et al. 2018](#)).

The detection of associated HI 21 cm absorption at high redshifts, $z > 1$, would allow one to extend the above studies to the early Universe and track the cosmological evolution of HI in AGN environments. Unfortunately, despite a number of searches (e.g. [Curran et al. 2008](#); [Aditya & Kanekar 2018a,b](#); [Grasha et al. 2019](#)), this endeavour remains

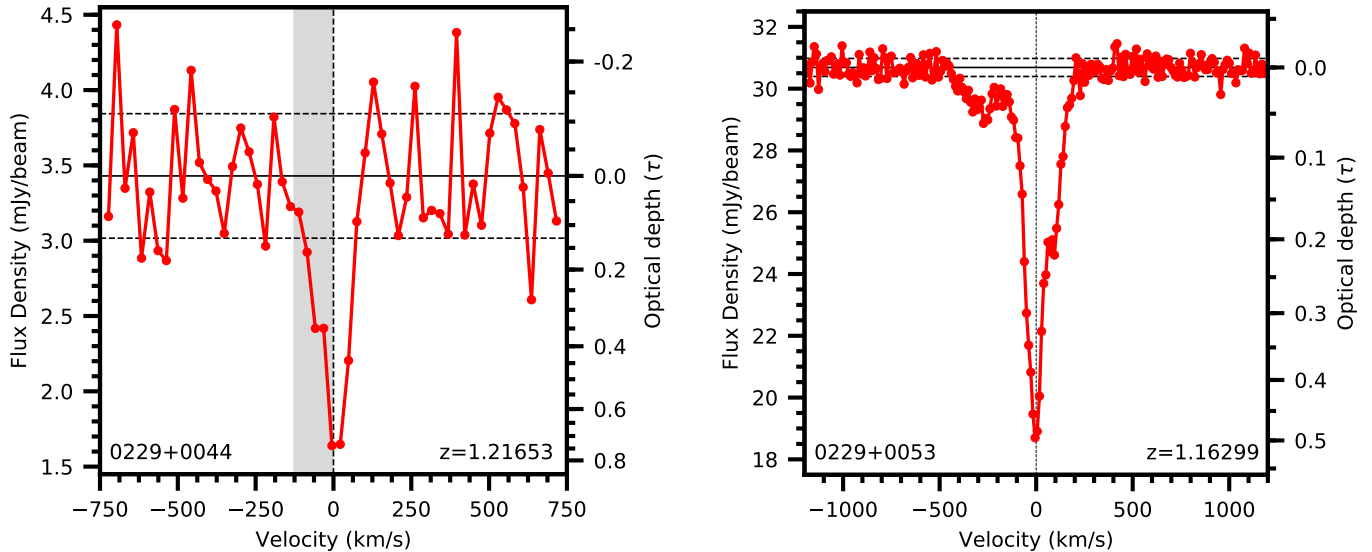


Figure 1. The HI 21 cm spectra towards [A] J0229+0044 and [B] J0229+0053, at velocity resolutions of $\approx 26.6 \text{ km s}^{-1}$ and $\approx 11.2 \text{ km s}^{-1}$, respectively. The solid horizontal line in each panel indicates the AGN continuum flux density at the redshifted HI 21 cm line frequency. The 1σ RMS noise values on the spectra (the horizontal dashed lines) are $0.41 \text{ mJy per } \approx 26.6 \text{ km s}^{-1}$ (J0229+0044) and $0.29 \text{ mJy per } \approx 11.2 \text{ km s}^{-1}$ (J0229+0053). The velocity axes in both panels are with respect to the redshift of the HI 21 cm absorption. The shaded region in the left panel indicates the optical spectroscopic redshift (and error) of J0229+0044, which is consistent with the HI 21 cm absorption redshift.

limited by the paucity of known high- z associated HI 21 cm absorbers. While more than a hundred such absorbers have been found at $z < 1$ (e.g. Vermeulen et al. 2003; Geréb et al. 2015; Maccagni et al. 2017; Aditya 2019), there are only 8 confirmed detections at $z > 1$ (Uson et al. 1991; Moore et al. 1999; Ishwara-Chandra et al. 2003; Curran et al. 2013; Aditya et al. 2017; Aditya & Kanekar 2018a; Dutta et al. 2020). Curran et al. (2008) argued that this apparent redshift evolution in the strength of the associated HI 21 cm absorption might arise because higher-redshift AGNs searched for HI 21 cm absorption typically have high ultraviolet (UV) and radio luminosities; however, their results were based on a heterogeneous AGN sample. This issue was further examined in an HI 21 cm absorption survey of a homogenous sample of flat-spectrum AGNs by Aditya & Kanekar (2018b), who found that associated HI 21 cm absorption is significantly weaker in AGNs at high redshifts, but also in AGNs with high rest-frame radio or ultraviolet (UV) luminosities. Unfortunately, the luminosity bias in their target sample, with high-luminosity AGNs at high redshifts, meant that it was not possible to break the above degeneracy between redshift evolution and AGN luminosity. Searches for associated HI 21 cm absorption in low-luminosity AGNs at high redshifts offer the best route to break this degeneracy.

Next, searches for associated HI 21 cm absorption have so far mostly been carried out in AGNs with known redshifts. This introduces a bias against AGN environments with high HI column densities, as such systems are likely to have high dust columns, which would obscure the AGN in the optical and UV wavebands, making it difficult to measure its redshift. HI 21 cm or mm-wave absorption surveys that target *all* radio AGNs independent of redshift information ensure no bias against dusty sightlines (e.g. Wiklind & Combes 1996; Kanekar et al. 2014a; Allison et al. 2015).

We have used the upgraded Giant Metrewave Radio Telescope (GMRT; Gupta et al. 2017) to carry out such an unbiased search for HI 21 cm absorption, covering the redshift range $z \approx 0.73 - 1.53$ against a large sample of radio sources. In this *Letter*, we report the discovery of two remarkable high-opacity HI 21 cm absorbers at $z \approx 1.2$, both identified against reddened AGNs, with low rest-frame radio and UV luminosities.

2. OBSERVATION, DATA ANALYSIS, AND RESULTS

The two new HI 21 cm absorbers were discovered in our 550 – 850 MHz survey of the DEEP2 Survey fields, using the Band-4 receivers of the upgraded GMRT. The DEEP2 Survey used the DEIMOS spectrograph on the Keck II Telescope to accurately measure the spectroscopic redshifts of 38,000 galaxies at $z \approx 0.70 - 1.45$, in four regions of the sky (Newman et al. 2013). Our GMRT survey used five pointings to cover two of the four DEEP2 field, with the

Table 1. HI 21 cm observational details and results. The columns are (1) the AGN name, (2) the J2000 co-ordinates, (3) the bandwidth, BW, in MHz, covering the HI 21 cm line, (4) the redshifted HI 21 cm line frequency, ν_{HI} , in MHz, (5), the RMS noise on the continuum image, in $\mu\text{Jy/Bm}$, (6) the AGN flux density at ν_{HI} , in mJy, (7) the original spectral resolution, ΔV , in km s^{-1} , (8) the RMS noise at the resolution ΔV , in mJy, (9) the velocity-integrated HI 21 cm optical depth, $\int \tau_{\text{HI}} dV$, in km s^{-1} , (10) the HI column density, N_{HI} , assuming $T_s = 100$ K and $f = 1$, and (11) the redshift of the peak of the HI 21 cm optical depth, z_{peak} .

AGN	Coordinates (J2000)	BW MHz	ν_{HI} MHz	σ_{cont} $\mu\text{Jy/Bm}$	S mJy	ΔV km s^{-1}	σ_{HI} mJy	$\int \tau_{\text{HI}} dV$ km s^{-1}	N_{HI} $\times 10^{22} \text{ cm}^{-2}$	z_{peak}
J0229+0044	02h29m28.9s, 00d44'29.5''	4.17	640.80	100	3.43 ± 0.38	3.8	0.87	74.2 ± 7.8	1.35 ± 0.14	1.2166
J0229+0053	02h29m47.2s, 00d53'08.9''	200	656.68	20	31.08 ± 0.41	5.6	0.41	78.41 ± 0.81	1.429 ± 0.015	1.1630

main aim of measuring the average HI mass of star-forming galaxies at $0.74 \leq z \leq 1.45$, by stacking the HI 21 cm emission spectra of galaxies with DEEP2 spectroscopic redshifts (Chowdhury et al. 2020). However, in addition to the primary science goal, the high spectral resolution of our survey ($\approx 18 - 25 \text{ km s}^{-1}$) allowed us to carry out an unbiased search for HI 21 cm absorption against all the (≈ 250) radio-continuum sources with flux densities ≥ 1 mJy (without correcting for the shape of the primary beam) in the five target fields, including sources without a known redshift. Our search was sensitive to both associated and intervening HI 21 cm absorption at $z \approx 0.73 - 1.53$. This search yielded the initial discovery of two high-opacity absorbers, at $z = 1.2166$ towards J0229+0044, and at $z = 1.1630$ towards J0229+0053, the focus of this *Letter*.

We followed up the two absorbers with GMRT Director’s Discretionary Time (DDT) in December 2019 (J0229+0044; proposal DDTC101) and February 2020 (J0229+0053; proposal DDTC121) to confirm the HI 21 cm absorption, and accurately measure the HI 21 cm optical depth. The total observing times were 10 hours (J0229+0044) and 12 hours (J0229+0053), using the GMRT Software Backend (GSB) and the GMRT Wideband Backend (GWB), respectively, as the primary correlator to cover the redshifted HI 21 cm line. The choice of correlator and the correlator settings were based on the aim of simultaneously covering the redshifted Lambda-doubled OH 18 cm lines; however, local oscillator tuning issues in the observations of J0229+0044 led us to a different correlator setup for the observations of J0229+0053. For J0229+0044, the OH 18 cm line frequencies were covered using the GWB as the secondary correlator, with a bandwidth of 200 MHz, centered at 700 MHz and sub-divided into 16,384 channels. Conversely, for J0229+0053, a single GWB 200 MHz band with 16,384 channels was used to cover both the HI 21 cm line and the OH 18 cm lines. The observational details (related to the HI 21 cm line) for the two sources are provided in Table 1.

The data were analyzed in the Common Astronomy Software Package (CASA version 5; McMullin et al. 2007), following standard procedures. The AOFLAGGER package (Offringa et al. 2012) was additionally used for excision of data affected by radio frequency interference (RFI). After the initial data editing, and gain and bandpass calibration using observations of the compact source 0204+152, a standard self-calibration procedure was carried out for each target source, using line-free channels. The imaging was done with the task TCLEAN, with the w-projection algorithm (Cornwell et al. 2008). In the case of J0229+0053, where the observing bandwidth was large, we additionally used the MT-MFS algorithm (second order expansion; Rau & Cornwell 2011) to image the target field. The synthesized beams of the final continuum images have full widths at half maximum (FWHMs) of $6.7'' \times 5.1''$ (J0229+0044) and $5.6'' \times 4.4''$ (J0229+0053). Both sources were found to be unresolved in our continuum images, with flux densities of (3.43 ± 0.38) mJy (J0229+0044, at ≈ 640 MHz) and (31.08 ± 0.41) mJy (J0229+0053, at ≈ 657 MHz). The quoted errors include the error measured from a 2-dimensional Gaussian fit to a small region around each source and the typical error in the GMRT flux density scale, $\approx 10\%$ at these frequencies.

The task UVSUB was then used to subtract out all detected continuum emission from the self-calibrated visibilities of each field. For each source, a spectral cube was made from these continuum-subtracted visibilities in the barycentric frame, using natural weighting. The HI 21 cm spectrum was extracted by taking a cut through the cube at the AGN location. The final spectrum for each source was then obtained by fitting a second-order polynomial to the line-free regions of each spectrum, and subtracting this out. We further smoothed the spectra by 7 channels (J0229+0044) and 2 channels (J0229+0053), to velocity resolutions of $\approx 26.6 \text{ km s}^{-1}$ and $\approx 11.2 \text{ km s}^{-1}$, respectively. The final optical depth RMS noise values are ≈ 0.12 per 26.6 km s^{-1} (J0229+0044) and 0.0068 per 11.2 km s^{-1} (J0229+0053).

Our final HI 21 cm spectra towards J0229+0044 and J0229+0053 are shown in Figs. 1[A] and 1[B], respectively. The velocity-integrated HI 21 cm optical depths are $(74.2 \pm 7.8) \text{ km s}^{-1}$ (J0229+0044) and $(78.41 \pm 0.81) \text{ km s}^{-1}$ (J0229+0053). Assuming $T_s = 100 \text{ K}$ and a covering factor, $f = 1$, these integrated HI 21 cm optical depths imply HI column densities of $N_{\text{HI}} = (1.35 \pm 0.14) \times (T_s/100) \times 10^{22} \text{ cm}^{-2}$ (J0229+0044) and $N_{\text{HI}} = (1.429 \pm 0.015) \times (T_s/100) \times 10^{22} \text{ cm}^{-2}$ (J0229+0053). Note that these are conservative assumptions: a lower covering factor or a higher spin temperature would imply even higher HI column densities. The observational results are summarized in Table 1.

Our correlator setup allowed us to carry out a simultaneous search for the redshifted OH 1665 MHz and 1667 MHz lines towards both sources (e.g. Kanekar & Chengalur 2002; Kanekar et al. 2005). The spectral RMS noise values at the redshifted OH line frequencies were 0.9 mJy/Bm per 9.7 km s^{-1} channel (J0229+0044) and 0.36 mJy/Bm per 9.5 km s^{-1} channel (J0229+0053); this yields 3σ upper limits to the velocity-integrated OH 1667 MHz optical depth of $\approx 9.5 \text{ km s}^{-1}$ (J0229+0044) and $\approx 0.25 \text{ km s}^{-1}$ (J0229+0053), assuming a Gaussian line profile with a line FWHM of 10 km s^{-1} .

3. THE AGNS: J0229+0044 AND J0229+0053

3.1. J0229+0044

The AGN J0229+0044 is spatially coincident with an object identified in the DEEP2 survey (DEEP2 42053345), with a spectroscopic redshift of $z = 1.2161 \pm 0.0045$ from the OIII λ 3727 doublet¹. The quasar has $g = 23.43 \pm 0.25$ from the Dark Energy Survey (DES; Abbott et al. 2018) and $K = 19.896 \pm 0.080$ from the ALHAMBRA survey (Moles et al. 2008), i.e. $g - K = 3.53 \pm 0.26$. The object is also detected by GALEX in the near-ultraviolet (NUV) band, with an NUV magnitude of 23.76 ± 0.22 (i.e. similar to the g-band magnitude); however, we note that the NUV-band emission may be contaminated by the Lyman- α emission of the AGN. We estimate the rest-frame 1215 Å luminosity² (L_{UV}) of J0229+0044 by interpolating between the measured B-band ($B = 23.516 \pm 0.058$; Willmer et al. 2006) and NUV magnitudes; this yields a 1215 Å luminosity of $L_{\text{UV}} = 10^{21.68} \text{ W Hz}^{-1}$ (this is formally an upper limit, due to the possibility that the GALEX NUV measurement may be affected by the AGN’s Lyman- α emission).

J0229+0044 has a 641 MHz flux density of $(3.43 \pm 0.38) \text{ mJy}$ in our GMRT continuum image; this implies a rest-frame 1.4 GHz radio luminosity of $L_{1.4 \text{ GHz}} = 10^{25.12} \text{ W Hz}^{-1}$. Further, the source has a flux density of 2.65 mJy at 1.4 GHz (from the VLA FIRST survey; Becker et al. 1995) and $1.55 \pm 0.07 \text{ mJy}$ at 8.5 GHz (from our analysis of an archival VLA X-band data set, project AC274). Combining the three measurements, we find that J0229+0044 has a relatively flat radio spectrum, with a spectral index of $\alpha \approx -0.3$ between 641 MHz and 8.5 GHz (where α is defined such that $S_\nu \propto \nu^\alpha$).

The HI 21 cm absorption towards J0229+0044, shown in Figure 1[A], consists of a single component, centered at $z = 1.216557 \pm 0.000058$. This is in excellent agreement with the spectroscopic redshift of the DEEP2 object, indicating that the HI 21 cm absorption arises from gas in the AGN environment. A single-component Gaussian fit to the HI 21 cm line profile yields a peak optical depth of $\tau_{\text{max}} = 0.727 \pm 0.083$ and an FWHM of $56.1 \pm 7.4 \text{ km s}^{-1}$. We emphasize that the optical depth sensitivity of the current GMRT HI 21 cm spectrum towards J0229+0044 is quite low, due to the low AGN flux density. We hence cannot rule out the presence of the wide associated HI 21 cm absorption that is typically detected in AGNs with $L_{1.4 \text{ GHz}} > 10^{24} \text{ W Hz}^{-1}$ (Maccagni et al. 2017).

3.2. J0229+0053

The HI 21 cm spectrum towards J0229+0053, shown in Fig. 1[B], has two distinct features: a strong component centred at $z = 1.16299$ and with a peak optical depth of ≈ 0.50 , and a wide weak wing that extends to $\approx -440 \text{ km s}^{-1}$ with respect to the main component. Unfortunately, the AGN does not currently have a spectroscopic redshift; its photometric redshift is $z = 0.86 \pm 0.22$ (Hsieh et al. 2005). The redshift of the main HI 21 cm component is in broad agreement with the AGN’s photometric redshift, but the large uncertainty in the photometric redshift means that we cannot formally rule out the possibility that the AGN is a background source (i.e. that the absorption arises from an “intervening” galaxy; e.g. Kanekar et al. 2014b). However, the high velocity-integrated HI 21 cm optical depth of the absorber suggests that it is likely to be an associated system; such high $\int \tau_{\text{HI}} dV$ values have hitherto only been obtained from HI 21 cm absorption in AGN environments (e.g. Geréb et al. 2015; Aditya & Kanekar 2018b; Kanekar

¹ The object was targeted in the DEEP2 survey at two different epochs and the DEEP2 catalog reports two redshifts, $z = 1.21639$ and $z = 1.21577$; these measurements are consistent within the $\approx 62 \text{ km s}^{-1}$ redshift error for redshift quality $Q = 3$ objects (Newman et al. 2013). We have used the mean of these two measurements as the AGN redshift, and have assumed the mean estimate to have a 1σ uncertainty of $\approx 62 \text{ km s}^{-1}$.

² We assume a flat Λ -cold dark matter cosmology, with $(H_0, \Omega_m, \Omega_\Lambda) = (70 \text{ km s}^{-1} \text{ Mpc}^{-1}, 0.3, 0.7)$ to convert flux densities to luminosity densities at the HI 21 cm absorption redshift.

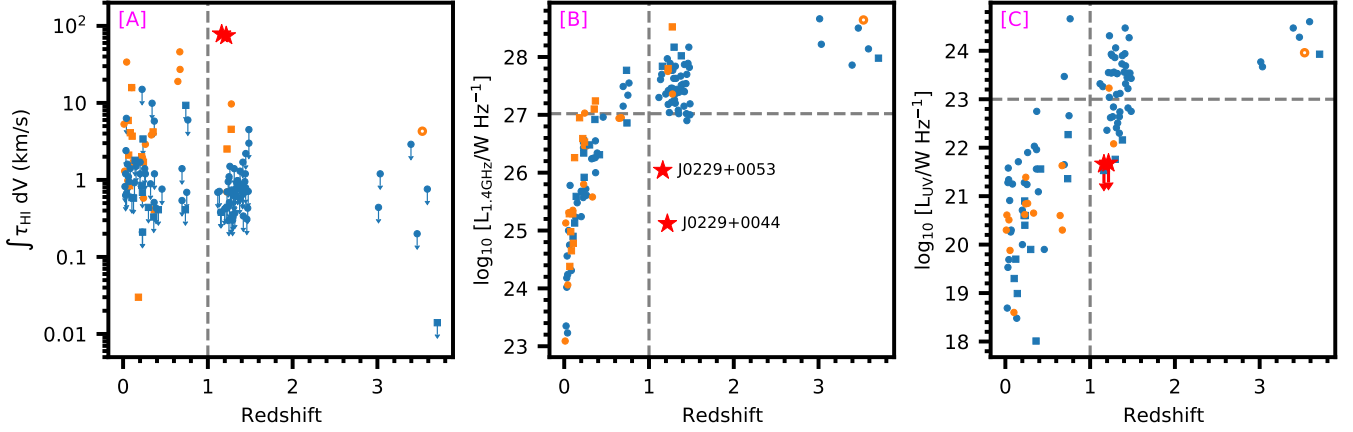


Figure 2. [A] The integrated HI 21 cm optical depth, [B] the rest-frame 1.4 GHz luminosity ($L_{1.4\text{GHz}}$), and [C] the rest-frame 1215 Å UV luminosity (L_{UV}), plotted against redshift, for flat-spectrum AGNs from the CJF sample (circles; Aditya & Kanekar 2018b), GPS sources (squares; Aditya & Kanekar 2018a), and the two sources of this *Letter* (red stars). Detections of HI 21 cm absorption in the CJF and GPS samples are shown in orange; for non-detections (shown in blue), the plotted velocity-integrated HI 21 cm optical depths are 3σ upper limits, assuming a line FWHM of 100 km s^{-1} . The open orange circle is a tentative detection of HI 21 cm absorption (Aditya et al. 2016). The horizontal dashed line in panel [B] marks the median $L_{1.4\text{GHz}}$ of the CJF and GPS samples, while that in panel [C] indicates $L_{\text{UV}} = 10^{23} \text{ W Hz}^{-1}$. See main text for discussion.

et al. 2014b). Further, the wide line profile, with $\Delta V \approx 640 \text{ km s}^{-1}$ between the nulls, is significantly larger than those seen in intervening systems, where $\Delta V \lesssim 200 \text{ km s}^{-1}$ (Kanekar et al. 2009). We hence conclude that the HI 21 cm absorption in J0229+0053 is likely to arise from gas in the AGN environment, i.e. that the AGN redshift is approximately equal to the HI 21 cm absorption redshift.

J0229+0053 is faint at ultraviolet and optical wavelengths, with $V = 24.09 \pm 0.16$, $B = 25.23 \pm 0.25$ (Hsieh et al. 2005), $g = 24.31 \pm 0.29$ (DES; Abbott et al. 2018), and a non-detection in the GALEX NUV band. The object is detected in the UKIDSS survey, with $K = 20.19 \pm 0.20$ (Lawrence et al. 2007). Interpolating between the B-band magnitude and the upper limit on the NUV magnitude yields the 3σ upper-limit $L_{\text{UV}} < 10^{21.66} \text{ W Hz}^{-1}$ on the 1215 Å luminosity, where we have assumed that the AGN redshift is the same as the HI 21 cm absorption redshift.

The measured GMRT 657 MHz flux density of $31.08 \pm 0.16 \text{ mJy}$ implies that J0229+0053 has a rest-frame 1.4 GHz luminosity of $L_{1.4\text{GHz}} = 10^{26.08} \text{ W Hz}^{-1}$, again assuming that the AGN redshift is the same as the HI 21 cm absorption redshift. The AGN has a flux density of $\approx 80.4 \text{ mJy}$ at 1.4 GHz (VLA FIRST survey; Becker et al. 1995), i.e. an inverted spectrum at low frequencies, with spectral index $\alpha \approx 1.3$. The AGN spectral index above 1.4 GHz is uncertain, due to inconsistencies between multiple 4.8 GHz flux-density measurements, $\approx 46 \text{ mJy}$ in the 87GB survey (Gregory & Condon 1991) and $\approx 100 \text{ mJy}$ in the MIT Green Bank 5 GHz survey (Bennett et al. 1986)³. These measurements yield spectral indices of $\alpha_{4.4\text{GHz}}^{1.4\text{GHz}} \approx -0.45$ or $= 0.18$. Thus, the AGN either is a GPS source or has an inverted spectrum at frequencies $\lesssim 5 \text{ GHz}$.

While the strength and width of the HI 21 cm absorption towards J0229+0053 imply that the absorption is likely to arise from gas in the AGN environment, a detailed understanding of the system critically requires a measurement of the AGN redshift. For example, if the AGN redshift is the same as the redshift of the main HI 21 cm absorption component, the wide and weak HI 21 cm absorption is likely to trace a jet-driven outflow of cold gas (e.g. Oosterloo et al. 2000; Morganti et al. 2013). Conversely, if the strong HI 21 cm absorption lies redward of the AGN redshift, the different HI 21 cm absorption components may arise against distinct sub-arcsecond-scale radio continuum structures (e.g. Peck & Taylor 2001; Struve et al. 2010).

4. DISCUSSION

The two new HI 21 cm absorbers presented here are remarkable due to both the faintness of the background sources, and the high velocity-integrated HI 21 cm optical depths, larger than that of any known redshifted HI 21 cm absorber

³ The discrepancy in the 4.8 GHz flux-density measurements could be due to either intrinsic variability or uncertainties in the flux density scale of the two surveys.

at $z > 0.2$ and nearly an order of magnitude higher than those at $z > 1$ (e.g. Curran et al. 2013; Aditya & Kanekar 2018a). Indeed, this is the first time that HI 21 cm absorption has ever been detected against a source with an integrated flux density lower than ≈ 25 mJy at the redshifted HI 21 cm line frequency at *any* redshift (e.g. Geréb et al. 2015; Maccagni et al. 2017; Aditya & Kanekar 2018b); J0229+0044 has a flux density of just ≈ 3.4 mJy! In passing, we note that VLBI HI 21 cm spectroscopy of low- z AGNs has yielded detections of HI 21 cm absorption against resolved source components with individual flux densities $\approx 3 - 10$ mJy (e.g. Józsa et al. 2009; Srianand et al. 2015), as well as similarly high HI 21 cm optical depths again against individual source components ($\int \tau_{\text{HI}} dV \approx 50 - 120 \text{ km s}^{-1}$; e.g. Morganti et al. 2004; Srianand et al. 2015).

Both AGNs show evidence for significant reddening, with $g-K = 3.53$ (J0229+0044) and $g-K = 4.12$ (J0229+0053). For comparison, only 0.2% of the 1,697 optically-selected QSOs at $z = 1.1 - 1.3$ in the SDSS-UKIDSS matched catalog of Peth et al. (2011) have $g-K > 2$, with none having $g-K > 2.5$. The inferred HI column density along the two sightlines is extremely high, $N_{\text{HI}} \approx 1.4 \times (T_s/100) \times 10^{22} \text{ cm}^{-2}$. This indicates a high dust column along the sightline, which is likely to cause high obscuration, and hence, reddening of the AGN (e.g. Webster et al. 1995). Searches for associated HI 21 cm absorption towards red quasars have shown higher detection rates, consistent with the hypothesis that the reddening is due to dust obscuration in the AGN environment (e.g. Carilli et al. 1998; Yan et al. 2016). However, it is possible that the apparent reddening might also arise due to the colour of the AGN host galaxy (e.g. Benn et al. 1998). Aditya & Kanekar (2018b) found no significant evidence of a dependence of the strength of HI 21 cm absorption on the AGN color, also suggesting that AGN reddening might arise from other causes.

We emphasize that the absorber towards J0229+0053 would not have been detected if we had limited our search to radio sources with known spectroscopic redshifts. Indeed, the detection of strong HI 21 cm absorption against J0229+0053, which is highly reddened and hence faint at optical and UV wavelengths, demonstrates the power of such unbiased searches in identifying high HI 21 cm opacity sightlines that are excellent candidates for molecular absorption.

Aditya & Kanekar (2018a,b) used HI 21 cm absorption surveys of GHz-peaked-spectrum (GPS) AGNs and flat-spectrum AGNs (the latter drawn from the Caltech-Jodrell Flat-spectrum (CJF) sample; e.g. Taylor et al. 1996), respectively, to find that associated HI 21 cm absorption is significantly weaker in AGNs at both high redshifts, and high rest-frame radio or UV luminosities. These associated HI 21 cm absorption studies are unique due to the homogeneity of the target AGN samples. Our two AGNs have flat or inverted low-frequency spectra, with radio spectral indices consistent with the spectral-index selection criterion ($\alpha \geq -0.5$) of the CJF sample⁴. Fig. 2[A] shows the velocity-integrated HI 21 cm optical depths of the 122 HI 21 cm absorbers of the CJF and GPS samples of Aditya & Kanekar (2018a,b) plotted as a function of redshift (with detections shown in orange and non-detections in blue). The low HI 21 cm absorption detection rate and the paucity of high-opacity absorbers at high redshifts are clear from the figure: there are only three confirmed HI 21 cm absorbers at $z > 1$, all with integrated HI 21 cm opacities $< 10 \text{ km s}^{-1}$. Figs. 2[B] and [C] illustrate the luminosity bias in the samples, with higher-redshift AGNs having higher radio and UV luminosities. The lower strength of associated HI 21 cm absorption in high-redshift AGNs of the GPS and CJF samples can hence be explained by (1) redshift evolution of the HI column density or gas spin temperature in AGN environments, (2) excitation of the upper hyperfine HI level due to the high AGN 1.4 GHz luminosity, resulting in a high spin temperature, or (3) ionization of the HI due to the high AGN UV luminosity, resulting in a low HI column density.

Our two new HI 21 cm absorbers are shown as red stars in each of the panels of Fig. 2. It is clear that they have far higher HI 21 cm optical depths, by nearly an order of magnitude, than any HI 21 cm absorber from the CJF or GPS samples at $z > 1$. Further, unlike all the CJF and GPS AGNs at $z > 1$, the two AGNs have relatively low luminosities in both the rest-frame 1.4 GHz and the UV wavebands, $L_{1.4 \text{ GHz}} = 10^{25.1} - 10^{26.08} \text{ W Hz}^{-1}$ and $L_{\text{UV}} \leq 10^{21.7} \text{ W Hz}^{-1}$. Our discovery of two high- z HI 21 cm absorbers with high velocity-integrated optical depths, and low rest-frame radio and UV AGN luminosities suggests that ionization and/or excitation effects play an important role in determining the strength of associated HI 21 cm absorption. It thus appears likely that the current paucity of HI 21 cm absorbers at $z > 1$ may be due to the luminosity bias in AGN samples that have so far been searched for associated HI 21 cm absorption.

⁴ We note that the spectral index of J0229+0053 is uncertain due to the difference between the two measurements of its 4.8 GHz flux density; however, the two 4.8 GHz measurements yield spectral indices ($\alpha = -0.45, +0.18$) consistent with the CJF selection criterion (see Section 3.2).

Of course, our results do not rule out the possibility of redshift evolution in AGN environments, in either the HI column density or the spin temperature. However, it is clear that tests of putative redshift evolution must be carried out on AGN samples with similar distributions of UV and radio luminosities, across a range of redshifts.

Finally, we note that the rest-frame 1215 Å luminosities of both J0229+0044 and J0029+0053 are significantly lower than the threshold of $L_{\text{UV}} = 10^{23} \text{ W Hz}^{-1}$ suggested by Curran et al. (2008), above which UV photons from the AGN may ionize most of the HI. Indeed, all the AGNs that show confirmed detections of associated HI 21 cm absorption at $z > 1$ have low rest-frame UV luminosities, $L_{\text{UV}} \lesssim 2 \times 10^{23} \text{ W Hz}^{-1}$ (Curran et al. 2008; Aditya et al. 2017; Aditya & Kanekar 2018a; Dutta et al. 2020), but show a wide dispersion in their rest-frame 1.4 GHz radio luminosities, $L_{1.4 \text{ GHz}} \approx 10^{25.1} - 10^{28.5} \text{ W Hz}^{-1}$. This suggests that the rarity of associated HI 21 cm absorbers at $z > 1$ may arise mainly because of a decrease in the HI column density in the AGN environment due to ionization of the HI by UV photons, rather than an increase in the HI spin temperature due to proximity to the bright radio AGN.

In summary, we have used an unbiased GMRT HI 21 cm absorption survey at $z \approx 0.73 - 1.53$ to discover two new HI 21 cm absorbers at $z \approx 1.2$, both of which are likely to arise from HI in the AGN environment. The two absorbers have the highest integrated HI 21 cm optical depths of all known redshifted HI 21 cm absorbers, with an inferred HI column density of $\approx 1.4 \times (T_s/100) \times 10^{22} \text{ cm}^{-2}$. Both AGNs are significantly reddened ($g-K = 3.53, 4.12$), consistent with dust obscuration at the above high HI column densities. The two AGNs have lower rest-frame 1215 Å UV and 1.4 GHz radio luminosities than most high- z AGNs that have hitherto been searched for HI 21 cm absorption. Our results suggest that ionization effects at high AGN UV luminosities are likely to play an important role in determining the strength of associated HI 21 cm absorption, and that the current dearth of HI 21 cm absorbers at $z > 1$ may be due to the luminosity bias in current high- z AGN samples with searches for HI 21 cm absorption. Unbiased HI 21 cm absorption surveys should allow us to significantly increase the number of HI 21 cm absorbers at high redshifts in the near future.

NK acknowledges support from the Department of Science and Technology via a Swarnajayanti Fellowship (DST/SJF/PSA-01/2012-13). The authors also acknowledge the Department of Atomic Energy for funding support, under project 12-R&D-TFR-5.02-0700. We thank the staff of the GMRT who have made these observations possible. The GMRT is run by the National Centre for Radio Astrophysics of the Tata Institute of Fundamental Research. It is a great pleasure for A.C. to thank Suma Murthy for numerous insightful discussions that led to the discovery of one of the absorbers reported in this *Letter*. A.C. also thanks Raffaella Morganti for a useful discussion on searching for associated HI 21 cm absorbers towards sources in the DEEP2 survey.

REFERENCES

- Abbott, T. M. C., Abdalla, F. B., Allam, S., et al. 2018, *ApJS*, 239, 18
- Aditya, J. N. H. S. 2019, *MNRAS*, 482, 5597
- Aditya, J. N. H. S., & Kanekar, N. 2018a, *MNRAS*, 473, 59
- . 2018b, *MNRAS*, 481, 1578
- Aditya, J. N. H. S., Kanekar, N., & Kurapati, S. 2016, *MNRAS*, 455, 4000
- Aditya, J. N. H. S., Kanekar, N., Prochaska, J. X., et al. 2017, *MNRAS*, 465, 5011
- Allison, J. R., Sadler, E. M., Moss, V. A., et al. 2015, *MNRAS*, 453, 1249
- Allison, J. R., Mahony, E. K., Moss, V. A., et al. 2019, *MNRAS*, 482, 2934
- Becker, R. H., White, R. L., & Helfand, D. J. 1995, *ApJ*, 450, 559
- Benn, C. R., Vigotti, M., Carballo, R., Gonzalez-Serrano, J. I., & Sanchez, S. F. 1998, *MNRAS*, 295, 451
- Bennett, C. L., Lawrence, C. R., Burke, B. F., Hewitt, J. N., & Mahoney, J. 1986, *ApJS*, 61, 1
- Carilli, C. L., Menten, K. M., Reid, M. J., Rupen, M. P., & Yun, M. S. 1998, *ApJ*, 494, 175
- Chowdhury, A., Kanekar, N., Chengalur, J. N., Sethi, S., & Dwarkhanath, K. S. 2020, *Nature*, Accepted
- Cornwell, T. J., Golap, K., & Bhatnagar, S. 2008, *IEEE Journal of Selected Topics in Signal Processing*, 2, 647
- Curran, S. J., Whiting, M. T., Tanna, A., et al. 2013, *MNRAS*, 429, 3402
- Curran, S. J., Whiting, M. T., Wiklind, T., et al. 2008, *MNRAS*, 391, 765
- Dutta, R., Raghunathan, S., Gupta, N., & Joshi, R. 2020, *MNRAS*, 491, 838
- Geréb, K., Maccagni, F. M., Morganti, R., & Oosterloo, T. A. 2015, *A&A*, 575, A44
- Grasha, K., Darling, J., Bolatto, A., Leroy, A. K., & Stocke, J. T. 2019, *ApJS*, 245, 3

- Gregory, P. C., & Condon, J. J. 1991, *ApJS*, 75, 1011
- Gupta, Y., Ajithkumar, B., Kale, H. S., et al. 2017, *Current Science*, 113, 707
- Hsieh, B. C., Yee, H. K. C., Lin, H., & Gladders, M. D. 2005, *ApJS*, 158, 161
- Ishwara-Chandra, C. H., Dwarakanath, K. S., & Anantharamaiah, K. R. 2003, *Journal of Astrophysics and Astronomy*, 24, 37
- Józsa, G. I. G., Garrett, M. A., Oosterloo, T. A., et al. 2009, *A&A*, 500, L33
- Kanekar, N. 2011, *ApJL*, 728, L12
- Kanekar, N., & Chengalur, J. N. 2002, *A&A*, 381, L73
- Kanekar, N., Ghosh, T., & Chengalur, J. N. 2018, *PhRvL*, 120, 061302
- Kanekar, N., Gupta, A., Carilli, C. L., Stocke, J. T., & Willett, K. W. 2014a, *ApJ*, 782, 56
- Kanekar, N., Prochaska, J. X., Ellison, S. L., & Chengalur, J. N. 2009, *MNRAS*, 396, 385
- Kanekar, N., Carilli, C. L., Langston, G. I., et al. 2005, *PhRvL*, 95, 261301
- Kanekar, N., Prochaska, J. X., Smette, A., et al. 2014b, *MNRAS*, 438, 2131
- Lawrence, A., Warren, S. J., Almaini, O., et al. 2007, *MNRAS*, 379, 1599
- Maccagni, F. M., Morganti, R., Oosterloo, T. A., Geréb, K., & Maddox, N. 2017, *A&A*, 604, A43
- McMullin, J. P., Waters, B., Schiebel, D., Young, W., & Golap, K. 2007, *Astronomical Society of the Pacific Conference Series*, Vol. 376, *CASA Architecture and Applications*, ed. R. A. Shaw, F. Hill, & D. J. Bell, 127
- Moles, M., Benítez, N., Aguerri, J. A. L., et al. 2008, *AJ*, 136, 1325
- Moore, C. B., Carilli, C. L., & Menten, K. M. 1999, *ApJL*, 510, L87
- Morganti, R., Fogasy, J., Paragi, Z., Oosterloo, T., & Orienti, M. 2013, *Science*, 341, 1082
- Morganti, R., & Oosterloo, T. 2018, *A&A Rv*, 26, 4
- Morganti, R., Oosterloo, T. A., Emonts, B. H. C., van der Hulst, J. M., & Tadhunter, C. N. 2003, *ApJL*, 593, L69
- Morganti, R., Oosterloo, T. A., Tadhunter, C. N., et al. 2004, *A&A*, 424, 119
- Morganti, R., Veilleux, S., Oosterloo, T., Teng, S. H., & Rupke, D. 2016, *A&A*, 593, A30
- Newman, J. A., Cooper, M. C., Davis, M., et al. 2013, *ApJS*, 208, 5
- Offringa, A. R., van de Gronde, J. J., & Roerdink, J. B. T. M. 2012, *A&A*, 539, A95
- Oosterloo, T. A., Morganti, R., Tzioumis, A., et al. 2000, *AJ*, 119, 2085
- Peck, A. B., & Taylor, G. B. 2001, *ApJL*, 554, L147
- Peth, M. A., Ross, N. P., & Schneider, D. P. 2011, *AJ*, 141, 105
- Rau, U., & Cornwell, T. J. 2011, *A&A*, 532, A71
- Srianand, R., Gupta, N., Momjian, E., & Vivek, M. 2015, *MNRAS*, 451, 917
- Struve, C., Oosterloo, T. A., Morganti, R., & Saripalli, L. 2010, *A&A*, 515, A67
- Taylor, G. B., Vermeulen, R. C., Readhead, A. C. S., et al. 1996, *ApJS*, 107, 37
- Uson, J. M., Bagri, D. S., & Cornwell, T. J. 1991, *PhRvL*, 67, 3328
- van Gorkom, J. H., Knapp, G. R., Ekers, R. D., et al. 1989, *AJ*, 97, 708
- Vermeulen, R. C., Pihlström, Y. M., Tschager, W., et al. 2003, *A&A*, 404, 861
- Webster, R. L., Francis, P. J., Petersont, B. A., Drinkwater, M. J., & Masci, F. J. 1995, *Nature*, 375, 469
- Wiklind, T., & Combes, F. 1994, *A&A*, 286, L9
- . 1996, *Nature*, 379, 139
- Willmer, C. N. A., Faber, S. M., Koo, D. C., et al. 2006, *ApJ*, 647, 853
- Yan, T., Stocke, J. T., Darling, J., et al. 2016, *AJ*, 151, 74